

This work was written as part of one of the author's official duties as an Employee of the United States Government and is therefore a work of the United States Government. In accordance with 17 U.S.C. 105, no copyright protection is available for such works under U.S. Law.

Public Domain Mark 1.0

<https://creativecommons.org/publicdomain/mark/1.0/>

Access to this work was provided by the University of Maryland, Baltimore County (UMBC) ScholarWorks@UMBC digital repository on the Maryland Shared Open Access (MD-SOAR) platform.

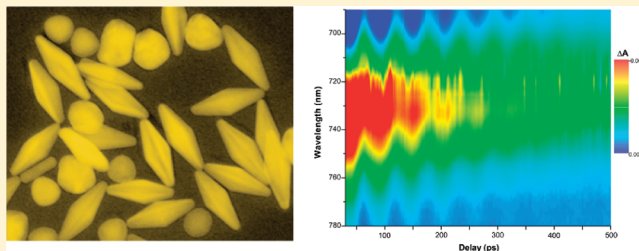
Please provide feedback

Please support the ScholarWorks@UMBC repository by emailing scholarworks-group@umbc.edu and telling us what having access to this work means to you and why it's important to you. Thank you.

Mechanical Damping of Longitudinal Acoustic Oscillations of Metal Nanoparticles in Solution

Matthew Pelton,^{*,†} Yiliang Wang,[†] David Gosztola,[†] and John E. Sader[‡][†]Center for Nanoscale Materials, Argonne National Laboratory, Argonne, Illinois 60439, United States[‡]Department of Mathematics and Statistics, The University of Melbourne, Victoria 3010, Australia

ABSTRACT: We present measurements and theoretical analysis of the damping of high-frequency acoustic vibrations of metal nanoparticles immersed in solution. Building on our previous work [Pelton, M.; Sader, J. E.; Burgin, J.; Liu, M.; Guyot-Sionnest, P.; Gosztola, D. *Nat. Nanotechnol.* **2009**, *4*, 492–495], we study several bipyramidal gold nanoparticle samples in a series of solvent environments in order to examine the origin of the measured damping. We use a fluid-structure interaction model to explain the damping due to the fluid surrounding the nanoparticles, extending the model to encompass the case of an arbitrary slender body. Good agreement with the theoretical model is found for a range of pure solvents and solvent mixtures, demonstrating that classical continuum theories for fluid mechanics are able to quantify high-frequency phenomena at the nanoscale. The remaining damping rate, which can be attributed to processes intrinsic to the nanoparticles, is consistent across all the measured samples. This demonstrates that the measured intrinsic damping is indeed a characteristic property of these bipyramidal metal nanoparticles, rather than being sample dependent.



I. INTRODUCTION

Nanomechanical devices have emerged as a versatile platform for a host of applications, including mass measurements with atomic-scale precision,^{1,2} detection of biomolecular interactions in fluid,³ and mass spectrometry.⁴ Central to the high sensitivity demonstrated in many of these applications is low mechanical energy dissipation.^{5,6} This ensures a resonance with a high quality factor, allowing for precise determination of changes in the resonant frequency and hence of analyte mass. The requirement for low mechanical losses has spurred extensive studies of energy dissipation as a function of device size, shape, material, and environment.^{5–9} Energy dissipation in many nanomechanical devices is measured by driving the devices externally or by monitoring their Brownian motion. These measurements are normally performed on nanoscale devices whose geometries are either one-dimensional, such as nanotube or nanobeam resonators,^{1,2,5} or two-dimensional, such as graphene sheets and nanoelectromechanical (NEMS) membranes.^{7,10} The mechanical motion of these devices can be monitored using standard electrical or optical techniques such as piezoresistive readout or optical interferometry.^{5,6} Such techniques, though, cannot be used to detect the motion of fully three-dimensional nanoscale structures such as colloidal metal nanoparticles, due to the difficulty in establishing electrical connections and the small sizes compared to optical wavelengths.

In addition, it is advantageous for many applications to be able to perform mass sensing in a liquid environment.^{3,11} In general, though, the surrounding fluid strongly damps the mechanical vibrations, greatly reducing the quality factor of the resonator and thus the detection sensitivity.^{5,8} Innovative structures have been

developed that overcome this problem by incorporating the liquid on the inside of the vibrating structure,^{9,11} but these designs cannot be straightforwardly extended to three-dimensional nanostructures.

By contrast, optical measurements on noble-metal nanoparticles provide the opportunity to study mechanical vibrations of three-dimensional objects in fluid environments. These optical studies are enabled by the surface plasmon resonances, or collective oscillations of conduction electrons, that such particles support. The plasmon resonances result in strong optical absorption and scattering when driven by incident light at their natural resonance frequency.¹² This frequency is sensitive to the dimensions of the nanoparticle and to the electron density, enabling time-domain optical measurements of acoustic oscillations in the particles.^{13–15} In such experiments, absorption of a short, pump laser pulse incident on the particles leads to rapid heating of the conduction electrons in the metal, which transfer their energy to the lattice on the time scale of a few picoseconds. This results in an isotropic thermal load within the particle on a time scale shorter than the natural vibration period, inducing nearly impulsive excitation of the vibrational modes in the nanoparticle. These vibrations, in turn, produce oscillations in the resonance frequency of surface plasmons supported by the nanoparticles, which are measured as changes in transmission of a second, probe laser pulse.

This method has been used for several years to measure vibration frequencies of metal nanoparticles, but measurements

Received: August 18, 2011

Revised: October 11, 2011

Published: October 19, 2011

of damping rates have proven more challenging. Typically, experiments involve large numbers of nanoparticles, which inevitably have variations in their sizes and shapes. This means that the particles all vibrate with slightly different periods, and the total signal decays due to dephasing. Early experiments on small spherical silver and gold particles in glass allowed the measurement of damping by the solid environment,¹⁶ but this was possible only because the damping was very rapid. In fluid environments, the environmental damping is slower and is typically overwhelmed by the inhomogeneous dephasing. Improvements in experimental techniques have made it possible to eliminate dephasing by making measurements on single particles;^{17–22} these measurements, though, have been somewhat difficult to interpret quantitatively, with large variations in damping rates being observed even among nominally identical nanoparticles from the same sample. This is related to the need to immobilize the nanoparticles on a substrate in order to make single-particle measurements, which results in a complex mechanical environment that can vary significantly from particle to particle. Single-particle measurements in a fluid environment may be possible by using optical tweezers to immobilize the particles,²³ but this will be a considerable challenge.

We recently reported a combined experimental and theoretical study of mechanical energy dissipation in a single sample of gold nanoparticles in pure solvent environments.²⁴ The measurements involved bipyramidal gold nanoparticles, synthesized using a recently developed method that results in exceptionally small variations in particle length.²⁵ The experiments were combined with a theoretical model to determine the losses due to viscous damping by the fluid that surrounds the particle, which we refer to as “fluid damping,” and any remaining losses that take place within the nanoparticle itself, which we refer to as “intrinsic damping.” One important question arises from this previous study: Is the measured intrinsic damping a general property of the nanoparticle geometry and material, or is it specific to the sample studied?

To answer this question, we report here the results of time-resolved optical experiments on several bipyramid samples. The fluid-structure model presented in ref 24 is also generalized to describe a slender body with arbitrary geometry, enabling monodisperse samples with different shapes and compositions to be studied. The model is found to be in quantitative agreement with the measured rates at which acoustic vibrations in the bipyramids are damped for a wide range of solvent environments, including both pure solvents and solvent mixtures. This agreement is achieved despite the nanometer-scale dimensions of the particles and the microwave frequencies of the mechanical vibrations. Our findings thus indicate that classical fluid and solid dynamics hold even under such extreme conditions. The extracted intrinsic damping is also found to be consistent across all samples measured. This indicates that the measured intrinsic damping is indeed a characteristic property of the nanoparticles, rather than being dependent on sample-dependent properties such as random crystal defects.

II. THEORETICAL MODEL FOR FLUID DAMPING

In this section, we present a theoretical model for a slender nanoparticle of arbitrary geometry in viscous fluid that is undergoing longitudinal oscillations, i.e., oscillations along the major axis of the nanoparticle, which is the dominant mode induced under ultrafast laser excitation.²⁶ This provides the essential

generalization of the model presented in ref 24, which was developed for bipyramidal particles only. It is assumed that the particle and fluid obey classic theories of linear elasticity and Newtonian fluid mechanics. The usual no-slip boundary condition is used at the interface between the solid and fluid.

We consider the formal asymptotic limit where the particle length greatly exceeds its width, i.e., $L \gg b$, where b is the maximum width of the particle and L is its length. This allows for the use of standard rod theory to describe longitudinal oscillations along the x -axis. An analogous formalism has previously been used to describe the flexural vibrations of cantilever beams in fluid.^{8,27}

The governing equation for the deformation, U , of the rod in the x -direction is²⁸

$$\frac{\partial}{\partial x} \left(EA \frac{\partial U}{\partial x} \right) - \rho_s A \frac{\partial^2 U}{\partial t^2} = - \int_{C_{\text{side}}} \mathbf{n}_s \cdot \boldsymbol{\sigma}_{\text{fluid}} \cdot \mathbf{i} \, dl \quad (1)$$

where $A(x)$ is the cross-sectional area of the rod, ρ_s is the particle density, $\boldsymbol{\sigma}_{\text{fluid}}$ is the stress tensor in the fluid, \mathbf{n}_s is a unit vector in the direction normal to the rod surface, $C_{\text{side}}(x)$ is the circumference of the cross section, and E is Young's modulus. Assuming a time dependence of $\exp(-i\omega t)$, where ω is the angular frequency of oscillation, we can immediately calculate the hydrodynamic force per unit length applied to the rod.

The viscous boundary layer over which vorticity diffuses from the solid surface is assumed to be thin in comparison to the nanoparticle diameter. (This will be the case for all our experimental results.) In this limiting case, a local plane analysis can be performed, whereby the flow at the surface is given by Stokes' second problem for the oscillation of a flat plate in an unbounded fluid.²⁹ From this classical solution, we readily obtain the hydrodynamic force per unit length:

$$\begin{aligned} F_{\text{hydro}} &= \int_{C_{\text{side}}} \mathbf{n}_s \cdot \boldsymbol{\sigma}_{\text{fluid}} \cdot \mathbf{i} \, dl \\ &= \mu \omega C_{\text{side}}(x) \sqrt{\frac{i\omega}{\nu}} u(x) \exp(-i\omega t) \end{aligned} \quad (2)$$

where $\nu = \mu/\rho$ is the fluid kinematic viscosity, μ is the fluid shear viscosity, ρ is the fluid density, and $u(x)$ is the spatial dependence of the displacement $U(x,t)$.

To determine the resonant frequency and damping due to the fluid, we calculate the Rayleigh quotient for eq 1. Scaling the x -direction by the length of the particle, L , substituting eq 2 into eq 1, and integrating over the entire particle length then yields

$$\begin{aligned} \bar{\omega}^2 &\equiv \left(\frac{L^2 \rho_s}{E} \right) \omega^2 \\ &= \frac{\int_{-1/2}^{1/2} A(x) (u'(x))^2 \, dx}{\int_{-1/2}^{1/2} \left(A(x) + \frac{\rho}{\rho_s} (1 + i) C_{\text{side}}(x) \sqrt{\frac{\nu}{2\omega}} \right) u^2(x) \, dx} \end{aligned} \quad (3)$$

Equation 3 specifies the complex angular frequency $\bar{\omega}$ in terms of the mode shape $u(x)$. This complex frequency can be used to determine the resonant frequency and quality factor (inverse scaled damping rate) of the fluid-structure problem.

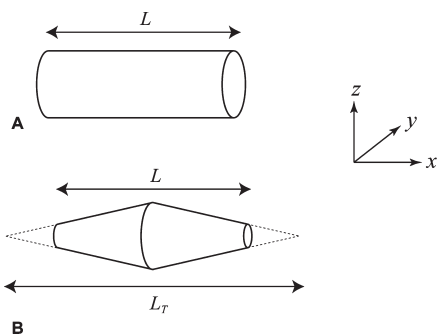


Figure 1. Schematics of modeled nanoparticles showing dimensions. The x -direction is along the length of the nanoparticle, with the origin situated at the midpoint between the ends. (A) Cylindrical particle; (B) bipyramidal particle. Both are shown with nominally circular cross sections. The length of the particle is L in both cases.

Next, we consider some examples of particles that are encountered in practice.

A. Cylindrical Particle. We first examine the case of a cylindrical particle of circular cross section and length L ; see Figure 1A. To calculate the resonant frequency and quality factor in fluid using eq 3, the mode shape of the deformation is required. Throughout, we approximate this by the mode shape of the rod in the absence of the fluid, i.e., in a vacuum. Using eq 1, the displacement mode shapes of extensional vibrations are given by²⁶

$$u(x) = \sin\left((2n + 1)\pi\frac{x}{L}\right) \quad (4)$$

where the mode number $n = 0, 1, 2, 3, \dots$ and the resonant frequencies in a vacuum are given by

$$\omega_{\text{vac}} = \frac{2n + 1}{L} \pi \sqrt{\frac{E}{\rho_s}} \quad (5)$$

For the fundamental mode ($n = 0$), eqs 3–5 yield

$$\bar{\omega}^2 \equiv \left(\frac{L^2 \rho_s}{E}\right) \omega^2 = \frac{\pi^2}{1 + (1 + i)\frac{\rho}{\rho_s} \sqrt{\frac{2\nu}{\omega R^2}}} \quad (6)$$

where R is the particle radius. The fundamental angular resonant frequency, ω_R , and quality factor in fluid, Q_{fluid} , follow immediately from eq 6:

$$\omega_R = \omega_{\text{vac}} [1 + \Gamma_{\text{cyl}}(\omega_R)]^{-1/2}, \quad Q_{\text{fluid}} = 1 + \frac{1}{\Gamma_{\text{cyl}}(\omega_R)} \quad (7)$$

where

$$\Gamma_{\text{cyl}}(\omega) = \frac{\rho}{\rho_s} \sqrt{\frac{2\nu}{\omega R^2}} \quad (8)$$

The quality factor is directly connected to the decay time τ of acoustic oscillations via the equation $Q = 2\omega_R \tau$.

B. Bipyramidal Particle. Next, we consider a bipyramidal particle. The lengths L and L_T are defined to be the actual and projected lengths of the particle, respectively; see Figure 1B. All lengths are now scaled by the projected length, L_T , rather than

the actual length, L , since this facilitates analytical evaluation. For simplicity, the cross section is again taken to be circular.

In this case, the mode shape of extensional vibrations in a vacuum is given by

$$u(x) = \frac{\sin\left(\Omega \frac{x}{L_T}\right)}{1 - \frac{2x}{L_T}} \quad (9)$$

where Ω is specified by the eigenvalue equation

$$\Omega \left(1 - \frac{L}{L_T}\right) \cos\left(\frac{\Omega L}{2L_T}\right) + 2 \sin\left(\frac{\Omega L}{2L_T}\right) = 0 \quad (10)$$

An asymptotic analysis of the solution to eq 10 yields the following explicit result for the fundamental mode:

$$\Omega = 2\pi + \frac{2\pi^3}{3} \left(1 - \frac{L}{L_T}\right)^3 + O\left[\left(1 - \frac{L}{L_T}\right)^4\right] \quad (11)$$

which establishes that the vacuum frequencies are weakly dependent on the ratio L/L_T . The fundamental resonant frequency is therefore well approximated by

$$\omega_{\text{vac}} = \frac{\Omega}{L_T} \sqrt{\frac{E}{\rho_s}} \approx \frac{2\pi}{L_T} \sqrt{\frac{E}{\rho_s}} \quad (12)$$

for many cases of practical interest.²⁴ Substituting eq 9 into eq 3 gives

$$\begin{aligned} \bar{\omega}^2 &\equiv \left(\frac{L_T^2 \rho_s}{E}\right) \omega^2 \\ &\approx \frac{4\pi^2}{1 + \left(2.44 - 9.87 \left[1 - \frac{L}{L_T}\right]^2\right) (1 + i) \frac{\rho}{\rho_s} \sqrt{\frac{2\nu}{\omega R_{\text{max}}^2}}} \\ &\quad + O\left[\left(1 - \frac{L}{L_T}\right)^3\right] \end{aligned} \quad (13)$$

where R_{max} is the maximum radius of the bipyramid particle.

The fundamental angular resonant frequency, ω_R , and quality factor in fluid, Q_{fluid} , can be obtained from eq 13:

$$\omega_R = \omega_{\text{vac}} [1 + \Gamma_{\text{bipyr}}(\omega_R)]^{1/2}, \quad Q_{\text{fluid}} = 1 + \frac{1}{\Gamma_{\text{bipyr}}(\omega_R)} \quad (14)$$

where

$$\Gamma_{\text{bipyr}}(\omega_R) = 2.44 \left(1 - 4.05 \left[1 - \frac{L}{L_T}\right]^2\right) \frac{\rho}{\rho_s} \sqrt{\frac{2\nu}{\omega R_{\text{max}}^2}} \quad (15)$$

C. Particle of Arbitrary Slender Shape. Particles of arbitrary slender shape can easily be studied using the above general formulation. All that is required is an exact or approximate solution for the vibrational mode for the particle in a vacuum. The resonant frequency and quality factor in fluid can then be determined directly from the Rayleigh quotient, eq 3.

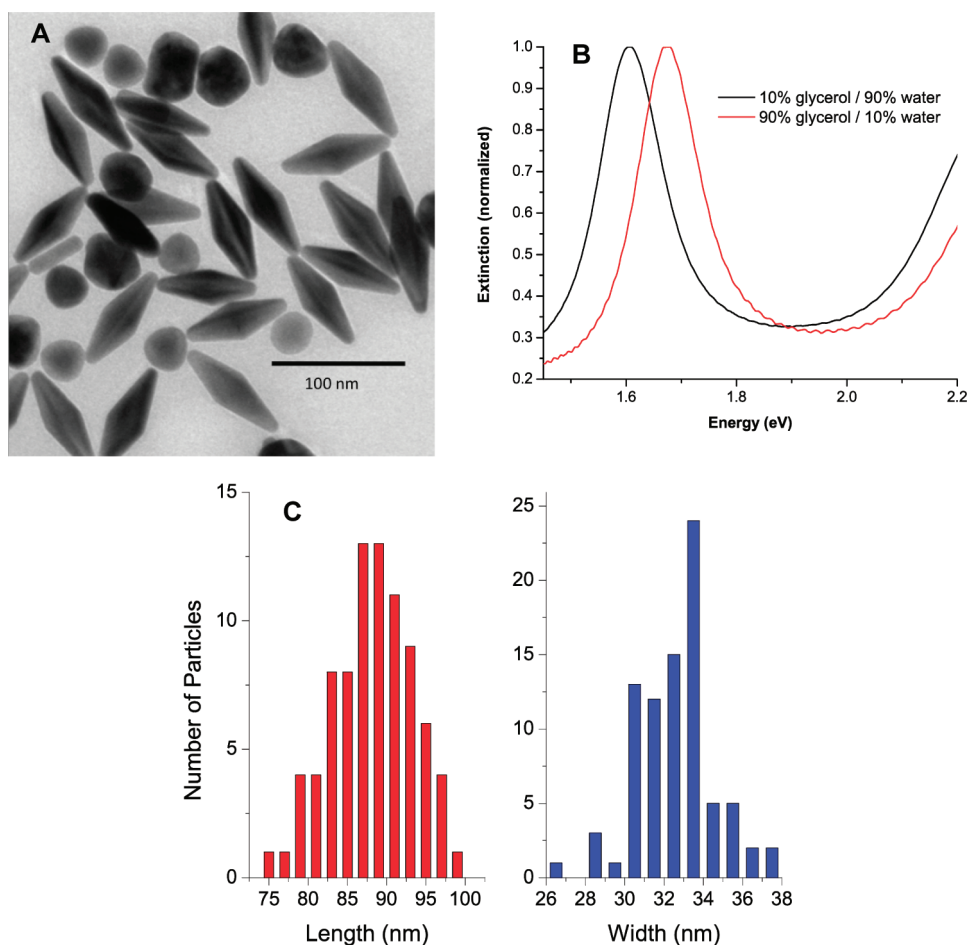


Figure 2. (A) Transmission-electron-microscope image of bipyramidal gold nanoparticles, together with an irregular, spheroidal biproduct. (B) Extinction spectra of the bipyramid sample in different solvent environments. The narrow peak is due to the longitudinal plasmon resonance in the bipyramids. (C) Histograms of lengths (from tip to tip) and widths (at the widest point) of bipyramids from the same sample.

We emphasize that the above theoretical model implicitly assumes that (i) the particle length greatly exceeds its width, and (ii) the hydrodynamic load is independent of frequency in the vicinity of the resonance, which is valid only if $Q_{\text{fluid}} \gg 1$.⁸ The latter requirement is consistent with the assumption of thin viscous boundary layers. In this limit, eqs 8 and 15 predict that the damping rate is proportional to $(\mu\rho)^{1/2}$; this scaling behavior is observed experimentally²⁴ (see below). Particles immersed in liquids with very high viscosity may deviate from this scaling behavior, since the viscous boundary thickness is proportional to the square root of the kinematic viscosity.²⁹

III. EXPERIMENTAL METHODS

A. Synthesis of Bipyramidal Gold Nanoparticles. Bipyramidal gold nanoparticles are produced using a seed-mediated growth method.²⁵ We start with rapidly nucleated gold seed nanoparticles, which form as decahedra with five twin boundaries. Gradual growth of the seeds from a solution of reduced gold salt results in nanoparticles that preserve the 5-fold symmetry without introducing additional crystal defects. When the growth is performed in the presence of silver ions, the particles have highly uniform bipyramidal shapes: standard deviations in the lengths of the particles can be as little as 2%,²⁴ and typical samples have standard deviations lower than 5%.

The seeds are produced by first preparing a 20-mL aqueous solution containing 0.125 mM HAuCl_4 and 0.25 mM sodium citrate. To this solution is quickly added, under vigorous stirring, 0.3 mL of freshly made, ice-cold 10 mM NaBH_4 . The resulting seed solution is aged at room temperature for 2 h before use. Following preparation of the seeds, stock solution for nanoparticle growth is produced by adding 1.5 mL of 10 mM HAuCl_4 and 0.24 mL of 0.01 M AgNO_3 to 30 mL of 0.1 M cetyltrimethylammonium bromide (CTAB) aqueous solution. The solution is then acidified with 0.6 mL of 1 N HCl , followed by addition of 0.24 mL of 0.1 M L-ascorbic acid to reduce the gold ions. Growth of the nanoparticles is initiated by adding 0.24 mL of the seed solution to this stock solution. The growth reaction proceeds at 30 °C for several hours, while the optical extinction spectrum of the solution is monitored. The reaction is completed when the spectrum shows a longitudinal plasmon peak at the desired frequency.

Figure 2A shows a transmission-electron-microscope (TEM) image of several particles from one such synthesis. The lengths and widths of approximately 75 bipyramids were measured from a series of such TEM images. The resulting distributions, shown in Figure 2C, are approximately Gaussian. A fit to this distribution thus provides the mean and standard deviation for the length and width of the bipyramids in this sample. Table 1 summarizes the results for this sample, labeled “sample 3,” as well as two additional samples; “sample 1” was previously described in ref 24.

Table 1. Dimensions and Corresponding Standard Deviations for Three Samples of Bipyramidal Gold Nanoparticles

	mean length (nm)	standard deviation in length (nm)	mean width (nm)	standard deviation in width (nm)
sample 1	77.7 ± 8.5	2.7 ± 0.3	27.8 ± 3.0	1.5 ± 0.2
sample 2	71.3 ± 11	4.6 ± 0.9	27.3 ± 4.4	1.2 ± 0.2
sample 3	89.1 ± 5.2	4.3 ± 0.2	32.6 ± 1.9	2.3 ± 0.1

In addition to the bipyramids, Figure 2A also shows the irregular, spheroidal particles that are produced as a byproduct of the synthesis procedure. The bipyramids exhibit a longitudinal plasmon resonance at relatively low frequencies, between approximately 1.6 and 1.7 eV, corresponding to conduction-electron oscillation along the long axis of the particles²⁵ (see Figure 2B). The byproduct, on the other hand, has a broad plasmon resonance at significantly higher frequencies, between 2.2 and 2.3 eV. By making measurements at frequencies around the longitudinal-plasmon resonance, then, it is possible to eliminate the effect of the byproduct, giving results that depend on the monodisperse bipyramids alone.

The bipyramids, as synthesized, are stabilized in aqueous solution by CTAB, a cationic surfactant. In order to transfer the sample to different solvent environments, we replace the CTAB with polystyrenesulfonic acid (PSS), a negatively charged polymer. The large excess of CTAB is first removed from the solution by cooling the sample solution in an ice–water bath for 1 h. The resulting CTAB crystals are removed by centrifuging the solution at 2000g for 15 min. The top solution is collected and centrifuged again, this time at 7000g for 6 min, so the metal nanoparticles are precipitated. The supernatant is removed, and the precipitated particles are redispersed in a solution of 0.03% PSS and 0.7 mM NaCl. After 1 h, excess PSS and NaCl are removed by centrifuging the sample at 7000g for 6 min and removing the supernatant. The precipitated particles are redispersed in a small volume of water, resulting in a concentrated aqueous solution. Small volumes of this solution are combined with various initial solvent mixtures in order to produce a solution of nanoparticles in a desired solvent environment. The final mixture is prepared in an optical cuvette with a path length of 2 mm. For all measurements, the final concentration of the bipyramids is adjusted such that the optical density at the longitudinal plasmon peak is between 0.2 and 0.3.

Figure 2B shows optical extinction spectra for sample 3 in two different solvent mixtures. The longitudinal plasmon frequency shifts because it is sensitive to the refractive index of the surrounding medium.¹² The line width remains unchanged, though, demonstrating that the sample is otherwise unaffected by the PSS functionalization and redispersion process.

B. Transient-Absorption Measurements. Acoustic vibrations in the bipyramids are measured using a transient-absorption-spectroscopy system (Ultrafast Systems HELIOS). Ultrafast pump laser pulses are incident on the sample, heating the nanoparticles and exciting acoustic vibrations. After a controllable time delay, a broadband probe pulse passes through the sample, and the probe transmission is measured as a function of wavelength. By comparing to the probe transmission in the absence of the pump pulse, a transient spectrum is obtained. This process is repeated for a range of delay times between the pump and probe, producing a two-dimensional map of differential probe transmission as a function of wavelength and delay time.

The pump and probe pulses are derived from the output of a regeneratively amplified Ti:sapphire laser (Spectra-Physics Tsunami

and SpitFire Pro), which produces pulses that are approximately 120 fs in duration at a repetition rate of 1.67 kHz. Ninety percent of the power from the amplified laser pulse is used to pump an optical parametric oscillator (OPA, Spectra-Physics TOPAS-C). The OPA produces the pump pulses, whose frequency is tuned to match the longitudinal plasmon resonance of the bipyramids. The pump power is adjusted using a variable neutral-density filter and is measured before the sample using a calibrated laser power meter. The pump beam is focused to a spot size of approximately 250 μm inside the sample cuvette. In order to avoid damage of the bipyramids, the average pump power is always kept at 150 μW or less.

The remaining 10% of the regenerative amplifier output is sent down a double-pass delay line consisting of a retroreflector on a motor-controlled stage and is then focused into a sapphire crystal. This results in a broadband probe pulse, which passes through an interference notch filter (Semrock NF03-808E-25) before being loosely focused onto the sample at the same spot as the pump. After passing through the sample, the probe is coupled through a multimode optical fiber into a spectrometer equipped with an array detector. The readout of the spectrometer is synchronized to the regenerative amplifier, allowing the spectrum of each probe pulse to be acquired by a control computer. The pump is modulated by a mechanical chopper, also synchronized to the amplifier, before arriving at the sample, so every second measurement of the probe spectrum is made while the pump is blocked. From the probe transmission spectra in the presence of the pump pulse, T_{on} , and in the absence of the probe pulse, T_{off} , the differential extinction $\Delta A = -\log_{10}(T_{\text{on}}/T_{\text{off}})$ is calculated. This value is averaged for 3 s for a particular time delay, resulting in one transient spectrum. The delay line is then moved, and the process is repeated for delay times from zero (corresponding to the pump and probe arriving at the sample simultaneously) to 500 ps in time steps of 2.5 ps. Two consecutive scans are averaged together to give the final data, and the results from the two scans are compared to each other in order to verify that the sample was not damaged or degraded during the measurement.

Thermal artifacts in the signal are typically avoided by stirring the sample with a magnetic stir bar, a strategy we have employed for relatively low viscosity fluids.²⁴ For many of the measurements reported here, though, the solvent mixtures used are too viscous for magnetic stirring to be effective. We therefore mount the sample cuvette on an automated translation stage that moves the sample during the measurements in a raster pattern at a speed of 1 mm/s.

A fraction of the pump laser power is scattered into the optical fiber that leads to the spectrometer. A background scattering signal is determined by averaging three spectra measured at negative time delays, and this intensity background is subtracted from all subsequent spectra. The portion of the scattering background that comes from the nanoparticle solution is effectively eliminated by this background-subtraction procedure, but the portion that comes from the surfaces of the cuvette varies over

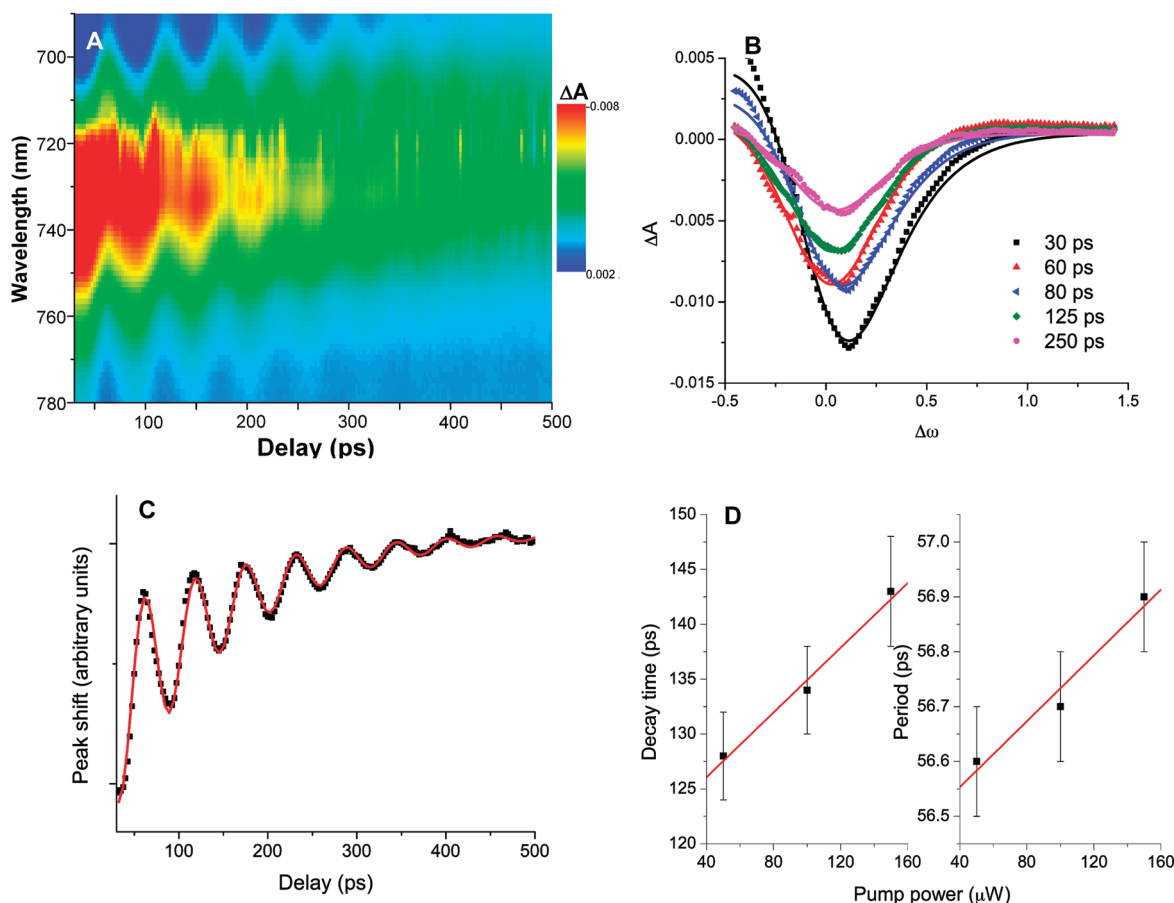


Figure 3. (A) Differential extinction, ΔA , for the same sample of bipyramidal gold nanoparticles as shown in Figure 1, as a function of probe wavelength and pump–probe delay. The data were measured using an average pump power of $150 \mu\text{W}$. The sample was in a mixture of 10% glycerol and 90% water by volume. (B) Sample transient-absorption spectra. The differential extinction is plotted against normalized frequency, $\Delta\omega \equiv \omega - \Omega_0/Z_0$, where ω is the probe frequency and Ω_0 and Z_0 are the plasmon resonance frequency and line width, respectively, in the absence of the pump pulse. Points are experimental data, and lines are fits to the difference of two Lorentzian functions, eq 16. (C) Shift in the frequency of the longitudinal surface plasmon resonance of the gold bipyramids as a function of time following excitation by a resonant pump laser pulse. The points are values determined by fitting the transient-absorption data, and the line is a fit to a damped oscillation plus an exponentially decaying background, eq 17. (D) Values of the decay time and period for acoustic vibrations in the gold bipyramids, determined by fitting the plasmon frequency shift as a function of pump–probe delay. The lines are linear fits as a function of pump power.

time as the sample is translated and cannot be subtracted completely.

Following the background subtraction, the measured signal is corrected for the fact that different probe wavelengths arrive at the focal spot at different times. A reference data set is collected on a sample of pure water, using the same pump and probe wavelengths as for the nanoparticle data, but using higher pump power. The water provides a nonresonant transient-absorption signal only when the pump and probe overlap. This signal is thus fitted in order to give the true time zero for various probe wavelengths, and time zero is determined for wavelengths between the fits by interpolation. The experimental spectra are offset by this measured offset for each wavelength.

C. Analysis of Transient-Absorption Data. A sample corrected data set is shown in Figure 3A. The plotted range of pump wavelengths covers only the longitudinal plasmon resonance peak of the bipyramidal particles, so the irregular byproduct does not contribute to the measured signal. The measured signal at any given pump–probe delay time can thus be attributed to a shift in the longitudinal plasmon resonance frequency of the bipyramids and a broadening of the plasmon resonance line. This

can be expressed in a simple mathematical form if the extinction spectra with and without the pump laser are both approximated as Lorentzian functions:³⁰

$$\Delta A \propto \frac{1}{\Delta\omega^2 + 1/4} - \frac{\gamma(t)}{[\Delta\Omega(t) - \Delta\omega]^2 + (1/4)[\gamma(t)]^2} \quad (16)$$

This expression involves the following normalized frequencies: $\Delta\omega \equiv \omega - \Omega_0/Z_0$, $\Delta\Omega(t) \equiv \Omega(t) - \Omega_0/Z_0$, and $\gamma(t) \equiv Z(t)/Z_0$, where ω is the probe frequency; $\Omega(t)$ and $Z(t)$ are the resonance frequency and line width, respectively, for a pump–probe delay t ; and Ω_0 and Z_0 are the plasmon resonance frequency and line width in the absence of the pump pulse. These last two values are determined by measuring the linear extinction spectrum of the bipyramid sample for each solvent environment (using a Perkin-Elmer Lambda 950 UV–vis spectrophotometer).

Sample transient spectra, in normalized frequency, and the corresponding best fits to eq 16 are shown in Figure 3B. The fits are performed only over the frequency range shown in the figure. The differences between the experimental spectra and the fits can

Table 2. Experimental Periods and Quality Factors for Acoustic Vibrations in Three Samples of Bipyramidal Gold Nanoparticles in a Variety of Fluid Environments, and Estimated Inhomogeneous Dephasing Times and Physical Properties of the Fluids

sample	inhomogeneous dephasing time T_{inh} (ps)	solvent	shear viscosity μ (cP)	density ρ (g/cm ³)	period T (ps)	quality factor Q_1
1	327 ± 33	methanol	0.54 ± 0.02	0.791	52.1 ± 0.3	17.3 ± 2.4
		water	0.89 ± 0.07	0.998	52.4 ± 0.8	15.7 ± 0.6
		ethylene glycol	16.1 ± 0.08	1.11	50.0 ± 1.5	8.6 ± 0.8
2	198 ± 17	10% glycerol in water	1.24 ± 0.06	1.02	47.1 ± 0.2	15.5 ± 2.6
		50% glycerol in water	4.5 ± 0.4	1.13	46.4 ± 0.4	8.7 ± 1.4
		70% glycerol in water	15.1 ± 1.7	1.17	44.1 ± 0.5	7.0 ± 1.2
3	263 ± 20	10% glycerol in water	1.24 ± 0.06	1.02	56.4 ± 0.2	14.5 ± 1.6
		20% glycerol in water	1.58 ± 0.08	1.04	56.5 ± 0.2	13.2 ± 1.4
		30% glycerol in water	2.1 ± 0.1	1.06	55.9 ± 0.2	11.5 ± 1.6
		60% glycerol in water	7.8 ± 1.8	1.14	55.0 ± 0.4	6.4 ± 0.9
		80% glycerol in water	39 ± 5	1.21	50.6 ± 1.1	4.1 ± 1.4

be attributed primarily to the assumption of a Lorentzian line shape: the small variation in the nanoparticle dimensions leads to an inhomogeneous broadening of the plasmon resonance, so the true line shape is a Voigt profile. The quality of the fits is also affected by the accuracy to which Ω_0 and Z_0 are determined; the effect of an error in these parameters is to increase the fitted peak shift while decreasing the fitted broadening or vice versa. In addition, the magnitudes of the fitted peak shift and broadening are sensitive to the magnitude of the measured transient-extinction signal, which depends on various experimental parameters such as the pump and probe focal spot sizes and the volume of their overlap zone. All of these effects, though, act identically on the fitted values for all time delays, which means that they do not affect the measured dynamics. We therefore consider only the peak shift, in arbitrary units, as illustrated in Figure 3C.

The time dependence of the peak shift, for pump–probe delays greater than 50 ps, consists of a damped oscillation on a decaying background. The background is due to the increased lattice temperature of the nanoparticles, which cools as heat is transferred to the solvent environment.^{31,32} The lattice cooling can be adequately described over this time range as a decaying exponential with time constant τ_{cool} . The oscillations are due to longitudinal acoustic vibrations of the bipyramids²⁴ and can be approximated as an exponentially damped sinusoid with period T and decay time T_{tot} . The peak shift can thus be described by the following function:

$$\Delta\Omega(t) = A_0 \exp\left(-\frac{t}{T_{\text{tot}}}\right) \sin\left(\frac{2\pi t}{T} + \phi\right) + A_1 \exp\left(-\frac{t}{\tau_{\text{cool}}}\right) \quad (17)$$

where A_0 , A_1 , and ϕ are fitting parameters. We fit the experimental peak shifts to eq 17 using a nonlinear least-squares fitting routine, as illustrated in Figure 3C. Since each parameter in eq 17 describes a different feature of the time response, tight fits are readily obtained.

The decay of the oscillations is due to the combination of inhomogeneous dephasing and energy decay. The inhomogeneous dephasing is strictly described by a Gaussian decay, provided the sample polydispersity follows a Gaussian distribution.²⁴ Approximating this by an exponential allows us to describe the total decay of the oscillating signal with a single decay time, T_{tot} , as is common in spectroscopy. In general, this

improves the stability of the nonlinear least-squares fitting, allowing the routine to converge on a reliable fit regardless of the starting parameters. In the cases where we were able to reliably describe the inhomogeneous dephasing with a Gaussian decay, we verified that the systematic error in the fitted decay rate introduced by the assumption of exponential decay is small compared to other sources of error.

The fitted decay rate and oscillation period are found to depend on pump power (see Figure 3D). The physical origin of this dependence is not entirely clear, but it may be caused by heating of the particle and solvent environment that results in a decrease in Young's modulus and solvent viscosity. Since the effect is relatively small, it is effectively eliminated by determining T and T_{tot} for several different pump powers and performing a linear regression to extrapolate to zero power.

IV. EXPERIMENTAL RESULTS AND DISCUSSION

As discussed above, the total experimental decay is due to the combination of inhomogeneous dephasing and energy decay:

$$\frac{1}{Q_{\text{tot}}} = \frac{1}{Q_{\text{inh}}} + \frac{1}{Q_1} \quad (18)$$

In eq 18, we express the various decay times in terms of the corresponding quality factors: Q_{tot} quantifies the experimental total decay, extrapolated to zero pump power, Q_{inh} is due to inhomogeneous dephasing, and Q_1 is due to energy decay.

The inhomogeneous dephasing depends only on the distribution of bipyramid dimensions, as listed in Table 1. In ref 24, we reported detailed finite-element simulations of the distribution of the oscillation periods in sample 1, based on dimensions of several nanoparticles measured from TEM images. Based on the mean, T_0 , and standard deviation, σ_T , of this distribution, we inferred an inhomogeneous damping time $T_{\text{inh}} \approx T_0^2/(\sqrt{2\pi}\sigma_T) = 327 \pm 33$ ps. According to eq 12, the oscillation period is expected to be approximately proportional to the projected bipyramid length L_T . Assuming that the distribution of L_T is approximately equal to the distribution of bipyramid lengths L , we obtain $T_{\text{inh}} \approx (T_0 L_0)/(\sqrt{2\pi}\sigma_L)$, where L_0 and σ_L are the mean and standard deviation, respectively, of the bipyramid length. Using the measured values from TEM images (see Table 1) and the measured period, we obtain $T_{\text{inh}} = 337 \pm 36$ ps, in good agreement with the value obtained by the laborious finite-element simulations. We therefore use this simple approximation to determine inhomogeneous damping times for the other two

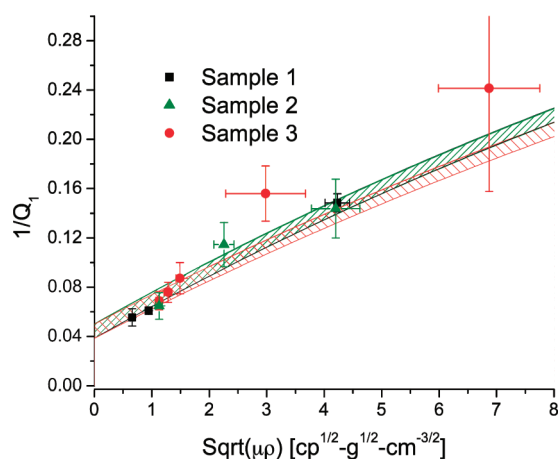


Figure 4. Relationship between the quality factor, Q_1 , for energy damping of acoustic vibrations in three different samples of bipyramidal gold nanoparticles and the shear viscosity, μ , and density, ρ , of the surrounding fluid. Points are experimentally measured values, and the hashed areas represent theoretical values, based on eqs 14 and 19, for intrinsic quality factors, Q_{int} , ranging from 20 to 26.

samples. The energy-decay quality factor, Q_1 , can then be determined using eq 18.

The resulting quality factors are listed in Table 2 for three different samples in a variety of solvent environments, together with the measured oscillation periods and relevant physical properties of the fluids. Glycerol–water mixtures are listed in terms of the volume percentage of glycerol in the total mixture. Viscosities and densities are obtained by interpolating between tabulated values,^{33,34} for a measured room temperature of 21 °C. Errors in the viscosities are estimated based on a temperature range of ± 2 °C.

We separate the total energy damping into a portion due to the surrounding fluid and the remaining damping, which can be attributed to processes intrinsic to the nanoparticle (including their surfaces):

$$\frac{1}{Q_1} = \frac{1}{Q_{\text{fluid}}} + \frac{1}{Q_{\text{int}}} \quad (19)$$

The quality factor Q_{fluid} is given by eq 14, which indicates that the quality factor should depend on the surrounding fluid only through the quantity $(\mu\rho)^{1/2}$, where μ is the fluid shear viscosity and ρ is its density. This expectation is confirmed experimentally, as shown in Figure 4.

The experimental data can be compared quantitatively to eqs 14 and 19 using Q_{int} as a single adjustable parameter. The bands plotted in Figure 4 show theoretical values for the range $Q_{\text{int}} = 23 \pm 3$. The bands for samples 1 and 2 are nearly identical, because of the similar sample dimensions. The experimental data for sample 3 appear to deviate somewhat from the theoretical predictions for higher solvent viscosities, which may represent a limitation of the simple theoretical model. Even so, it is striking that the measured intrinsic quality factors of all three samples are identical, to within experimental error. This demonstrates that the measured intrinsic damping is not specific to any individual sample but is a general property of the material and geometry. We note that, in this context, the nanoparticles include both their gold core and their PSS shells, and intrinsic damping processes

may be occurring within either of the materials or at the interface between the two of them.

The fitted value of $Q_{\text{int}} = 23 \pm 3$ should be greater than the quality factor that would be measured for a single particle immobilized on a substrate, since the single particle would also experience dissipation to the solid environment. Vibrations in single gold bipyramids have not yet been measured, but several other metal nanoparticles have. For 10-nm gold spheres in a polymer film on a glass substrate, values of Q from 15 to 30 were measured;¹⁷ for gold nanoprisms evaporated onto a glass slide, Q varied from 6 to 28;²⁰ for silver nanocubes in a polymer film on a glass substrate, Q varied from 7 to 12.¹⁹ On the other hand, single gold nanorods with dimensions comparable to the bipyramids studied here gave $Q = 29 \pm 9$,¹⁸ suggesting that the intrinsic damping in the nanorods is less than that in the bipyramids. The nanorods were deposited onto a glass substrate from CTAB-stabilized solution; much of the CTAB may come off the nanorod surfaces when they are deposited, resulting in nearly bare gold surfaces. The bipyramids in solution, by comparison, are coated with a layer of PSS, which may introduce further damping at the metal–polymer interface or within the polymer shell. In addition, the bipyramids have five twinning planes running along their length, whereas the nanorods can be free of boundary planes.²⁵ The crystallinity of nanoparticles has been observed to affect their vibration periods,³⁵ so it is not unreasonable to expect that twin boundaries could produce additional damping of the vibrations. On the other hand, any random defects in the nanoparticles, distinct from these built-in twinning planes, would be expected to vary from sample to sample. The fact that we measure identical intrinsic damping among the three samples studied allows us to rule out any such sample-dependent structural defects as the source of the damping.

V. CONCLUSIONS

Using exceptionally monodisperse bipyramidal samples, we have measured the damping rates for acoustic vibrations of gold nanoparticles in fluid environments. In particular, we investigated whether there is any difference in intrinsic damping of different samples of the same type of nanoparticle. We observed that this damping component is identical, within experimental error, for three samples of bipyramidal gold nanoparticles. This provides strong evidence that the intrinsic damping is a characteristic property of the material and geometry, rather than being dependent on specifics of the sample and its preparation.

We also provided the essential extension of our previous theoretical model for fluid damping²⁴ to long, slender nanoparticles of arbitrary shape. This generalized model requires only the mode shape of the particle in the absence of fluid, which can be easily obtained by solving the thin rod equation. For the measurements performed here, the portion of the damping due to the surrounding fluid is in good quantitative agreement with this analytical model for the three different samples studied in a wide range of solvents and solvent mixtures. This provides confirmation that classical continuum theories for fluid and solid mechanics are able to quantify high-frequency phenomena at the nanometer scale.

The mechanisms responsible for the measured intrinsic damping remain uncertain. In particular, it is unclear why the measured damping rate for our bipyramidal samples appears to be faster than damping rates for gold nanorods based on single-particle measurements. It would therefore be of great value to

extend the measurements to metal nanoparticles with different internal structures and with different surface properties, in order to quantify their role in the damping processes. Obtaining appropriate samples with sufficiently small variation in their dimensions will require continuing advances in nanoparticle synthesis. Synthesis of monodisperse samples with dimensions comparable to the gold bipyramids but made of other materials would provide further insight into the intrinsic damping mechanisms. Alternatively, extension of the measurements to complex and non-Newtonian fluids would allow for a unique investigation of fluid dynamics at small dimensions and on short time scales.

AUTHOR INFORMATION

Corresponding Author

*Tel.: (630) 252-4598. Fax: (630) 252-4646. E-mail: pelton@anl.gov.

ACKNOWLEDGMENT

We thank Mingzhao Liu, Philippe Guyot-Sionnest, and Julien Burgin for their essential contributions to earlier stages of this project. Work at the Center for Nanoscale Materials was supported by the U.S. Department of Energy, Office of Science, Office of Basic Energy Sciences, under Contract No. DE-AC02-06CH11357. J.E.S. acknowledges support from the Australian Research Council Grants Scheme.

REFERENCES

- (1) Chiu, H.-Y.; Hung, P.; Postma, H. W. Ch.; Bockrath, M. *Nano Lett.* **2008**, *8*, 4342–4346.
- (2) Jensen, K.; Kim, K.; Zettl, A. *Nat. Nanotechnol.* **2008**, *3*, 533–537.
- (3) Lavrik, N. V.; Sepaniak, M. J.; Datskos, P. G. *Rev. Sci. Instrum.* **2004**, *75*, 2229–2253.
- (4) Naik, A. K.; Hanay, M. S.; Hiebert, W. K.; Feng, X. L.; Roukes, M. L. *Nat. Nanotechnol.* **2009**, *4*, 445–449.
- (5) Ekinici, K. L.; Roukes, M. L. *Rev. Sci. Instrum.* **2005**, *76*, 061101.
- (6) Craighead, H. G. *Science* **2000**, *290*, 1532–1535.
- (7) Barton, R. A.; Ilic, B.; van der Zande, A. M.; Whitney, W. S.; McEuen, P. L.; Parpia, J. M.; Craighead, H. G. *Nano Lett.* **2011**, *11*, 1232–1236.
- (8) Sader, J. E. *J. Appl. Phys.* **1998**, *84*, 64–76.
- (9) Sader, J. E.; Burg, T. P.; Manalis, S. R. *J. Fluid Mech.* **2010**, *650*, 215–250.
- (10) Bunch, J. S.; van der Zande, A. M.; Verbridge, S. S.; Frank, I. W.; Tanenbaum, D. M.; Parpia, J. M.; Craighead, H. G.; McEuen, P. L. *Science* **2007**, *315*, 490–493.
- (11) Burg, T. P.; Godin, M.; Knudsen, S. M.; Shen, W.; Carlson, G.; Foster, J. S.; Babcock, K.; Manalis, S. R. *Nature* **2007**, *446*, 1066–1069.
- (12) Pelton, M.; Aizpurua, J.; Bryant, G. W. *Laser Photonics Rev.* **2008**, *2*, 135–169.
- (13) Hodak, J. H.; Henglein, A.; Hartland, G. V. *J. Phys. Chem. B* **2000**, *104*, 9954–9965.
- (14) Voisin, C.; Del Fatti, N.; Christofilos, D.; Vallée, F. *J. Phys. Chem. B* **2001**, *105*, 2264–2280.
- (15) Hartland, G. V. *Annu. Rev. Phys. Chem.* **2006**, *57*, 403–450.
- (16) Voisin, C.; Christofilos, D.; Del Fatti, N.; Vallée, F. *Physica B* **2002**, *316–317*, 89–94.
- (17) van Dijk, M. A.; Lippitz, M.; Orrit, M. *Phys. Rev. Lett.* **2008**, *95*, 267406. van Dijk, M. A.; Lippitz, M.; Stolwijk, D.; Orrit, M. *Opt. Express* **2007**, *15*, 2273–2287.
- (18) P. Zijlstra, P.; Tchegbotareva, A. L.; Chon, J. W. M.; Gu, M.; Orrit, M. *Nano Lett.* **2008**, *8*, 3493–3497.

- (19) Staleva, H.; Hartland, G. V. *J. Phys. Chem. C* **2008**, *112*, 7535–7539. Staleva, H.; Hartland, G. V. *Adv. Funct. Mater.* **2008**, *18*, 3809–3817. Staleva, H.; Skrabalak, S.; Carey, C.; Kosel, T.; Xia, Y.; Hartland, G. V. *J. Phys. Chem. Chem. Phys.* **2009**, *11*, 5889–5896.
- (20) Burgin, J.; Langot, P.; Del Fatti, N.; Vallée, F.; Huang, W.; El-Sayed, M. A. *J. Phys. Chem. C* **2008**, *112*, 11231–11235.
- (21) Guillet, Y.; Rossignol, C.; Audoin, B.; Calbris, G.; Ravaine, S. *Appl. Phys. Lett.* **2009**, *95*, 061909.
- (22) Hartland, G. V. *Chem. Sci.* **2010**, *1*, 303–309.
- (23) Pelton, M.; Liu, M.; Kim, H. Y.; Smith, G.; Guyot-Sionnest, P.; Scherer, N. F. *Opt. Lett.* **2006**, *31*, 2075–2077.
- (24) Pelton, M.; Sader, J. E.; Burgin, J.; Liu, M.; Guyot-Sionnest, P.; Gosztola, D. *Nat. Nanotechnol.* **2009**, *4*, 492–495.
- (25) Liu, M.; Guyot-Sionnest, P. *J. Phys. Chem. B* **2005**, *109*, 22192–22200.
- (26) Hu, M.; Wang, X.; Hartland, G. V.; Mulvaney, P.; Juste, J. P.; Sader, J. E. *J. Am. Chem. Soc.* **2003**, *125*, 14925–14933.
- (27) van Eysden, C. A.; Sader, J. E. *J. Appl. Phys.* **2007**, *101*, 044908.
- (28) Love, A. E. H. *A Treatise on the Mathematical Theory of Elasticity*; Dover Publications: New York, 1944.
- (29) Batchelor, G. K. *An Introduction to Fluid Dynamics*; Cambridge University Press: Cambridge, U.K., 1967.
- (30) Seferyan, H. Y.; Zadayan, R.; Wark, A. W.; Corn, R. A.; Apkarian, B. A. *J. Phys. Chem. C* **2007**, *111*, 18525–18532.
- (31) Hu, M.; Hartland, G. V. *J. Phys. Chem. B* **2002**, *106*, 7029–7033.
- (32) Wilson, O.; Hu, X.; Cahill, D.; Braun, P. *Phys. Rev. B* **2002**, *66*, 224301.
- (33) *CRC Handbook of Chemistry and Physics*, 89th ed.; Lide, D. R., Ed.; CRC Press: Boca Raton, FL, 2008.
- (34) Physical properties of OPTIM Glycerine published by The Dow Chemical Company. Available at <http://www.dow.com/glycerine/resources/physicalprop.htm>.
- (35) Tang, Y.; Ouyang, M. *Nat. Mater.* **2007**, *6*, 754–759.